CHAPTER 15

PRESERVATION OF THE TRANSVERSE EMITTANCE

15.1 INTRODUCTION

The brightness of the nominal LHC proton beam (i.e. the ratio between the bunch population and its emittance) is significantly higher than that of the other multi-bunch beams produced so far by the accelerators of the LHC injector chain. Only the bunches produced for the $p\bar{p}$ collider period had similar transverse and longitudinal brightness, however the total intensity of this beam was almost two orders of magnitude smaller than that of the nominal LHC beam. On the other hand, the beam for SPS fixed-target physics [1] has a total intensity comparable to the LHC ultimate beam, but its longitudinal and transverse brightness are far smaller. The LHC imposes a very tight transverse emittance blow-up budget: the SPS as LHC injector [2] has to deliver a beam with a normalised rms transverse emittance of at most 3.5 μm, while receiving a 3.0 μm beam from the PS.

Control of the transfer of the LHC beam from the PS to the SPS is critical for emittance preservation. The transfer is performed by fast extraction from the PS into the transfer line TT2-TT10 which connects the PS and SPS. The beam is then single-turn injected into the SPS. In the present filling scheme it is planned to have up to four injections per SPS cycle (see Chap. 12). In the SPS other potential sources of emittance growth come into play, including single-particle phenomena, such as resonances and transverse instabilities. When the SPS as LHC injector project [2] was launched the resistive wall instability was thought to be the main additional cause of transverse instabilities. However, during machine developments studies with the LHC beam in the SPS it became evident that coupling between the beam and the electron cloud it creates is in fact the dominant mechanism responsible for transverse instabilities. In this respect, the mechanisms and cures for emittance blow-up have had to be significantly reviewed.

15.2 THE TT2-TT10 TRANSFER LINE FROM PS TO SPS

The injection transfer line consists of two parts: the TT2 line (formerly used to transfer beam from the PS to the ISR) and the TT10 line, which branches off the TT2 line about 320 m downstream from the PS extraction. The TT2 line consists of a FODO lattice with a period length of about 18.5 m and a phase advance per cell of almost 30° in the horizontal plane and 50° in the vertical plane. The focussing and defocusing quadrupole families are independently powered. The FODO section is located downstream of a matching section, which consists of seven independently powered quadrupoles. An additional quadrupole, which is also independently powered, is installed just upstream of the switching dipoles to TT10. This quadrupole is downstream of the thin foil which is used to strip the ion beams for fixed target physics in the SPS experimental areas.

The TT10 line includes the switching magnets that bend the beam horizontally in the direction of the SPS (by 196 mrad) and the four vertical dipoles grouped in pairs of opposite strength. These dipole pairs are used to lower the beam by 32 m from TT2 down to the level of the SPS ring. The long distance transfer (about 800 m) consists of a FODO lattice, similar to that of the SPS machine. The FODO section has a period length of about 60.5 m and a phase advance per cell of almost 90° in the horizontal plane and 75° in the vertical plane. The matching between the lattices of TT2 and TT10 is made using a matching section located between the two FODO structures. This section consists of six independently powered quadrupoles (in addition to the single quadrupole at the end of TT2) and two independently powered interleaved doublets. The beta function and dispersion of the injection line are shown in Fig. 15.1.

15.3 STATIC INJECTION ERRORS

Detailed linear optical models exist for both the PS and SPS machines as well as for the injection transfer lines [3,4,5,6]. These models have been verified with beam based measurements and proved to reproduce the observations accurately [7,8,9]. The most difficult part of the model is the simulation of the optics as seen by the beam at extraction from the PS. Here the beam traverses a region where the fringe fields from the combined function main magnets is are rather strong. For the LHC beam, this phenomenon is particularly

important, since at the extraction momentum of 26 GeV/c, the PS magnets are well into saturation and the fringe fields are strongest.

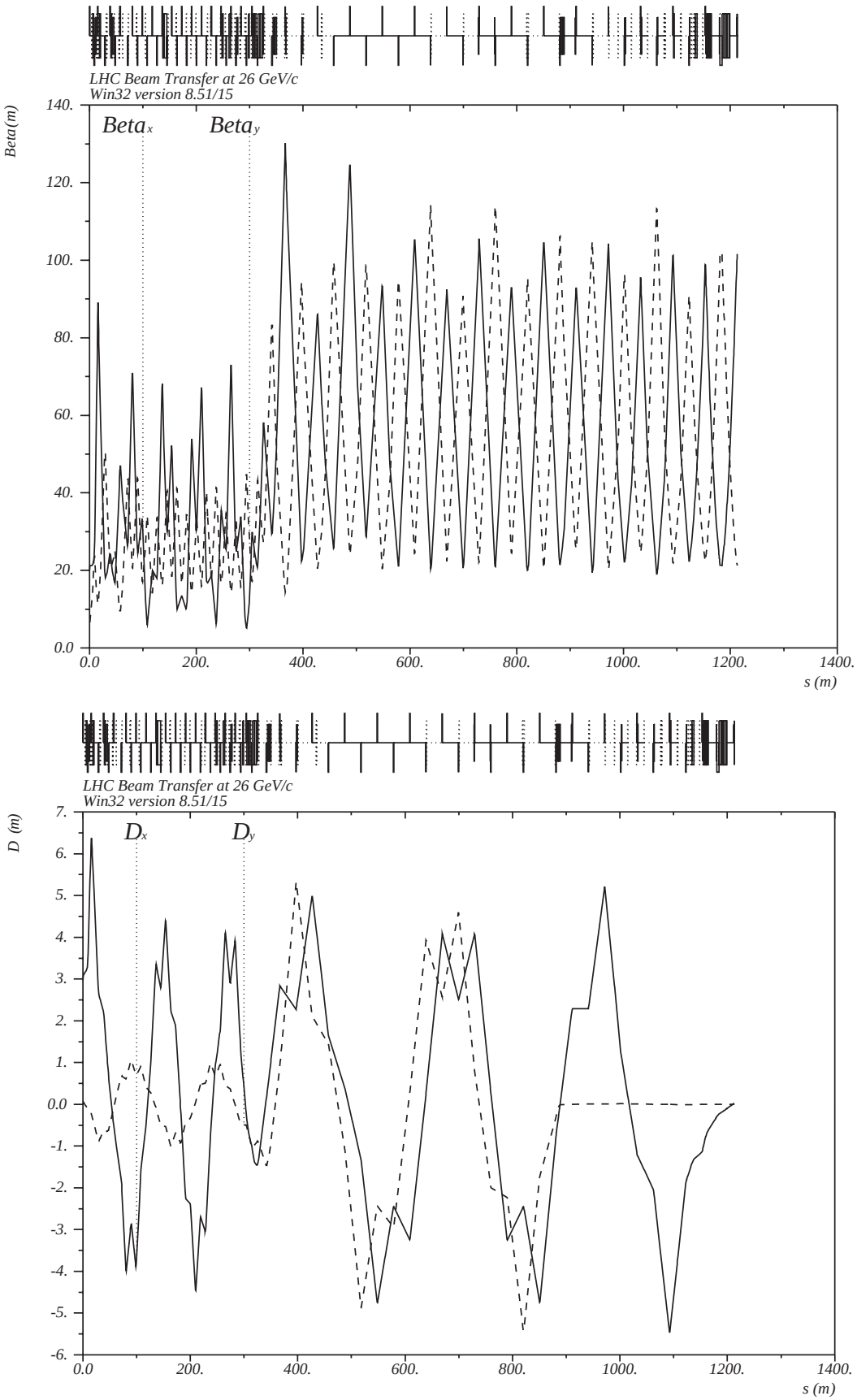

Figure 15.1: Beta (top) and dispersion (bottom) functions for the transfer line TT2-TT10.

Model calculations [10,11] of the PS magnet fringe fields which match the observations fairly well have been made, however, some uncertainties persist. Any uncertainties in the optical parameters of the extracted beam will propagate through the transfer line. In addition, other uncertainties coming from energy errors, together with magnet alignment and bending and quadrupole errors in the line must be taken into account. The combination of all error sources will lead to the following static errors on the beam:

- Injection errors
- Dispersion mismatch
- Betatron mismatch

Each of these errors, if not corrected, will provoke an increase in the transverse distribution of the beam because of filamentation. This occurs in all circular machines because of the presence of non-linear magnetic fields or electromagnetic phenomena, such as space-charge. The density of the core of the distribution is almost unaffected by these errors, but beam tails are created. The resulting dilution of the beam or the corresponding reduction of its brightness can be quantified by the so-called emittance blow-up after filamentation ($\Delta\varepsilon_{af}$) [12], though this is a pessimistic representation of the loss in brightness. Each of the main error sources and its contribution to emittance blow-up is described below.

15.3.1 Injection Errors

Injection errors are the deviations in position and angle (Δx, $\Delta x'$) of the injected beam at the injection point with respect to the closed orbit of the machine at the same point. The emittance increase $\Delta\varepsilon_{af}$ due to injection errors is given by:

$$\Delta\varepsilon_{af} = \frac{\Delta X_n^2 + \Delta X_n^{'2}}{2}$$

where (ΔX_n, $\Delta X'_n$) are the normalised quantities corresponding to the above errors. The effects of injection errors are more severe for smaller values of the transverse emittance of the beam because of the additive nature of this source of emittance growth. These errors can be corrected down to the resolution of the observation system. For the SPS this resolution has a σ of 70 μm in the horizontal and 24 μm in the vertical plane [13]. Hence, correction at these levels implies a normalised emittance blow-up of:

$$\Delta\varepsilon^*_{af,H(V)} = \beta\gamma\frac{\sigma^2_{H(V)}}{\beta_{H(V)}} \approx 1.4\times10^{-3}\ \left(1.6\times10^{-4}\right)\ \mu\text{m}$$

where $\beta_{H,V}$ (~100 m) are the horizontal and beta functions at the ring beam position monitors used for the correction of the injection oscillations and β and γ are the relativistic factors at injection. This contribution is completely negligible even for the beams with a very small normalised emittance (ε^* =1 μm).

15.3.2 Dispersion Mismatch

Dispersion mismatch at the injection point in the SPS is an additional source of emittance blow-up. This arises since off-momentum particles will be injected with a position and angle error with respect to the corresponding off-momentum closed orbit. They will then undergo betatron oscillations around that orbit in the SPS ring. While the injection error resulting from the average momentum offset can be corrected in a way similar to injection errors, the error experienced by each off-momentum particle cannot be corrected individually and will therefore result in a distortion of the beam distribution and in tails [12]. This phenomenon is particularly strong for the nominal LHC beam since it has a large momentum spread and small transverse emittance. For other types of LHC beam it can be even stronger, since some have a very small transverse emittance.

The emittance blow-up factor due to dispersion mismatch (ΔD, $\Delta D'$) is given by:

$$J_D = 1 + \frac{\left(\Delta D_n^2 + \Delta D'^2_n\right)\sigma^2_{\delta p/p0}}{2\varepsilon}$$

where (ΔD_n, $\Delta D_n'$) are the normalised dispersion and dispersion derivative errors at the injection point while $\sigma_{\delta p/p0}$ and ε are the rms momentum spread and rms emittance of the beam, respectively.

The dispersion at the end of the transfer line depends on the value at the exit of the PS. The two matching sections can be used to match the actual dispersion to the required values at the injection point in the SPS.

The initial conditions for the dispersion and its derivative at extraction from the PS and the dispersion mismatch can be determined by measuring the dispersion in the transfer line and on the first turn in the SPS ring, which is here considered as a continuation of the transfer line. The measurement of the dispersion is performed by varying the momentum of the beam extracted from PS in steps and recording the transverse displacement at each available beam position monitor. The momentum offset Δp with respect to the reference momentum p_0 is calculated by measuring the change in radial position ΔR of the beam in the first turn and by applying the relation:

$$\frac{\Delta p}{p_0} = \frac{1}{\alpha_p}\frac{\Delta R}{R}$$

This procedure requires the knowledge of the radius R of the SPS machine and the momentum compaction factor α_p both have been measured quite precisely (see Tab. 15.2) [14,15]. A pencil beam (both in transverse and longitudinal emittance) must be used in order to avoid losses for large relative momentum offsets (a few 10-3) and to improve resolution. The typical parameters of such a beam are listed in Tab. 15.1.

Table 15.1: Parameters of the beam used for dispersion and dispersion mismatch measurements

Bunch intensity [10^{11} protons]	0.4
Number of bunches	1
Longitudinal emittance [eV.s]	0.16
Rms. momentum spread [10^{-3}]	0.2
Rms. bunch duration [ns]	2.5
Rms. normalised transverse emittance (H/V) [μm]	3 / 3

Additional beam position monitors have been added in the TT2 and TT10 lines. Previously, only secondary emission monitors were installed in TT2. In the TT10 line the additional monitors have been placed in such a way as to increase the overall accuracy of the measurement. The existing and newly installed monitors have been equipped with a low frequency acquisition system [16] in order to measure the long bunches of the beam. The method used takes advantage of the large number of beam position monitors in the SPS ring and provides an immediate picture of the mismatch with respect to the dispersion in the ring. Any deviation of the dispersion measured over the first turn from the SPS dispersion is an indication of a dispersion mismatch and potential emittance blow-up.

The measurement procedure is well suited for machine setup at the beginning of the run or in case of problems. The experience gained so far has shown that the precision of the measurement is better than 10 % in the initial values of the dispersion and its derivative [17,18]. This corresponds to a potential emittance blow-up factor of the order of 10% for the nominal LHC beam.

15.3.3 Betatron Mismatch

The mismatch between the beta functions at the end of the TT2-TT10 transfer line and those of the SPS machine at the injection point is an additional source of emittance blow-up. Once again a major source of difficulty is the uncertainty in the extraction conditions from the PS.

The corresponding blow-up factor after filamentation H is given by:

$$H = \frac{1}{2}\left[\frac{\beta_0}{\beta_m} + \frac{\beta_m}{\beta_0} + \left(\alpha_0\sqrt{\frac{\beta_m}{\beta_0}} - \alpha_m\sqrt{\frac{\beta_0}{\beta_m}}\right)^2\right]$$

In the above equation α_0 and β_0 are the expected Twiss parameters, while α_m and β_m are the measured ones. Unlike dipole injection errors and dispersion mismatch, the effect of a betatron mismatch on emittance is multiplicative. Hence the relative blow-up does not depend on the initial emittance. Betatron mismatch can be determined by measuring the beam size at three or more beam profile monitors per plane. This is valid if the momentum spread of the beam, the dispersion at the monitors and the transfer matrices between any pair of monitors are known ([17] and references therein). The emittance ε of the beam and the Twiss parameters α and β at any of the beam profile monitors can be derived from this measurement. The Twiss parameters can also be inferred at any other point in the line (and in particular at the PS extraction point) providing that the transfer matrix to that point is known.

The following secondary emission (SEM) monitors are installed in the transfer lines:

- Two SEM wire monitors (MSF257, MSF277) with a spacing of 0.5 mm,
- One SEM wire monitor (MSF267) with a spacing of 0.3mm,
- Three SEM grids with a pitch of 2.5 mm (MSG258, MSG268, MSG278) in TT2,
- Three SEM grids with a pitch of 2.5 mm (BSG102737, BSG102837, BSG102937) in TT10.

These monitors were normally used for the measurements of the profile of the fixed target beam however, the SEM grids do not have sufficient resolution to provide an accurate measurement of the emittance and hence the Twiss parameters, given the small beam size of the LHC beam. The pitch of the SEM grids coincides with the rms beam size and therefore only a few strips are intercepted by the beam. Furthermore, SEM monitors cannot be used with the LHC nominal beam because of the strong background signal induced on the grids by electron multipacting during the beam passage [19].

For these reasons five Optical Transition Radiation (OTR) screens have been installed in the injection line, one in TT2 and four in TT10. The OTR screens are imaged by CCD cameras and the optics collecting the transition radiation is of such a quality that resolutions of the order of 150 μm can be achieved [20]. Using the above monitors, the precision obtained in the Twiss parameters at the PS extraction point is of the order of 10% [17,18]. This corresponds to an emittance blow-up factor of a few percent for the nominal LHC beam.

15.3.4 Other Sources of Static Injection Errors

Any deviation of the beam momentum from the nominal value used to compute the settings of the magnetic elements of the line might also induce a non-negligible mismatch at injection [17]. The circumference of the SPS machine (corresponding to the length of the beam orbit going through the centre of all the ring beam position monitors) has been measured [14,15] and the injection momentum of the beam has been determined from the RF frequency at SPS injection. The corresponding values are listed in Tab. 15.2 for a perfect energy matching between PS and SPS.

Table 15.2: Beam momentum at injection for a perfect energy matching between PS and SPS.

SPS circumference [m]	6911.5542 ± 0.0094
RF frequency at injection [Hz]	200264560 ± 1
Harmonic number	4620
Beam momentum [GeV/c]	25.99 ± 0.03

Cross-plane coupling in the TT2-TT10 transfer line or in the PS machine at the extraction energy might be an additional source of emittance growth at injection in the SPS where coupling is corrected down to the 10-3 level using the closest tune approach. If coupling is present, non-vanishing XY cross terms appear in the

four-dimensional beam covariance matrix M_{4D} and the term ρ provides the expected blow-up factor after filamentation due to beam coupling.

$$\rho = \left(\frac{\det M_X \, \det M_Y}{\det M_{4D}} \right)^{1/4}$$

where M_X and M_Y are the two-dimensional sub-matrices in the horizontal and vertical planes [21].

Coupling in the injection line can also be generated by misalignments of dipole or quadrupole magnets in the form of tilts. The presence of coupling in the injection line can be measured by comparing the trajectories of a pencil beam (see Tab. 15.1) for different corrector excitations. Measurements have excluded the presence of significant localised sources of coupling in the injection line [21].

Once the presence of sources of coupling in the injection line is excluded, coupling at the extraction from the PS machine can be monitored using profile measurements made with the OTR screens in the injection line as these provide the two-dimensional beam distribution in space. This method is described in [21] and is an extension (including beam coupling) of that described in [22]. Each OTR monitor provides three constraints to the measurements (the correlations <XX>, <YY> and <XY>). The 15 independent elements of the 5 × 5 beam covariance matrix can be measured if at least 5 OTR screens are available. The number of fitting parameters and therefore the number of constraints reduces to 11 if no betatron-momentum correlation is assumed and if the dispersion is well known (from the measurement described in the Sect. 15.3.2). If the momentum spread of the beam is known the number of fitting parameters can be reduced to 14 and 10, respectively.

Using the precise knowledge of the dispersion in the transfer line the 11-parameter or 10-parameter fits have been applied to measurements made in the line. Though the available OTRs provide enough constraints, during the measurements more than one optics were loaded (typically three) in order to provide extra-redundancy for the fit [21]. An unmistakeable coupling term originating in the PS ring has been measured and indirectly confirmed by measurements performed in the PS ring at 26 GeV/c [23]. The expected mismatch due to measured coupling in the PS is of the order of a few percent. In the same way as for the estimated betatron and dispersion mismatch, this is a somewhat pessimistic estimate of the induced emittance growth.

The TT2-TT10 transfer line is equipped with three skew quadrupoles powered in series which are used for fixed-target operation. However, these are located in the TT10 matching section and their use for the LHC beam would reduce the number of free parameters available for betatron and dispersion matching to the SPS. Therefore it is preferable to correct the coupling in the PS ring itself.

Non-linear fields at extraction might result in a dependence of the initial conditions on the extraction trajectory and on the extraction energy. Presently there are no non-linear magnetic elements installed in the injection line to compensate for such non-linear phenomena.

15.3.5 Optical Parameters at Extraction from PS

During 2001 and 2002 a series of measurements was performed in order to precisely determine the initial conditions for the injection line. This measurement series included the dependence of the Twiss parameters and the dispersion together with its derivative on the momentum offset [24]. The results of these measurements are shown in Figs. 15.2 and 15.3. The corresponding blow-up factors have been estimated from the measurements and are shown in Fig. 15.4. The estimated blow-up factors are only marginally dependent on the estimated momentum offset in the interval $\pm 2 \times 10^{-3}$ that is relevant for the LHC beam assuming a parabolic momentum distribution.

The PS extraction point is defined to be the entrance of the quadrupole QFO105. The initial conditions at this point for the nominal momentum are listed in Tab. 15.3.

The estimated blow-up factor after filamentation is 40% in the horizontal plane and 5% in the vertical plane in the range of momenta $\pm 2 \times 10^{-3}$. As previously mentioned, this represents a pessimistic estimate of the core emittance growth.

Table 15.3: Measured initial conditions at the PS extraction point for the nominal momentum.

	Horizontal	**Vertical**
β [m]	22.8	6.77
α [1]	-2.18	0.419
D [m]	3.06	0.090
D'[1]	0.346	-0.029

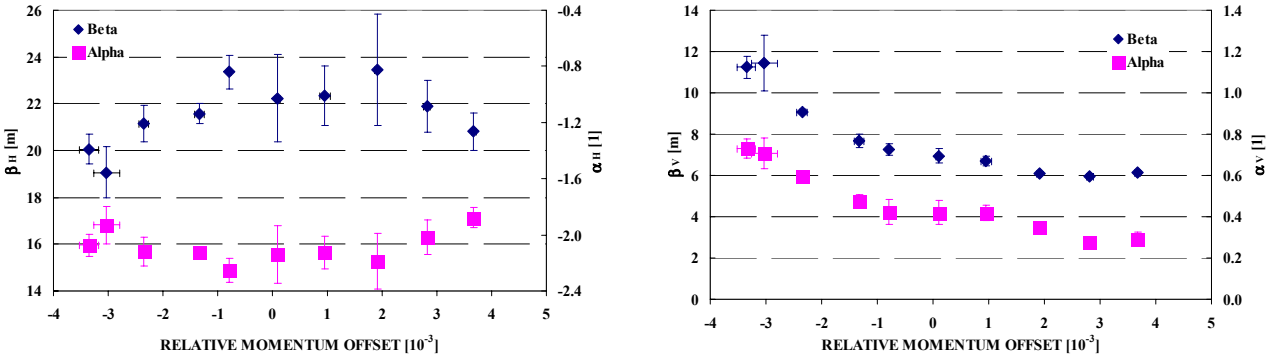

Figure 15.2: Horizontal (left) & vertical (right) β values at the PS extraction point vs. momentum offset.

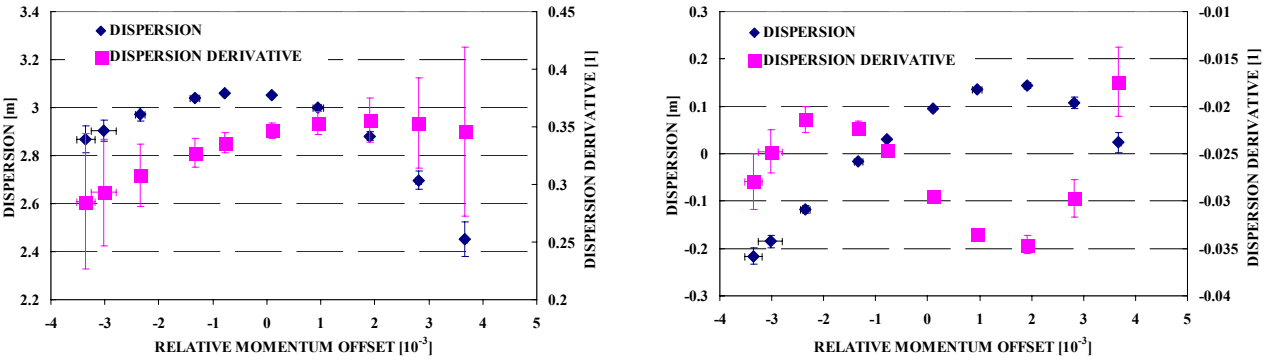

Figure 15.3. Horizontal (left) & vertical (right) D and D' at the PS extraction point vs. momentum offset.

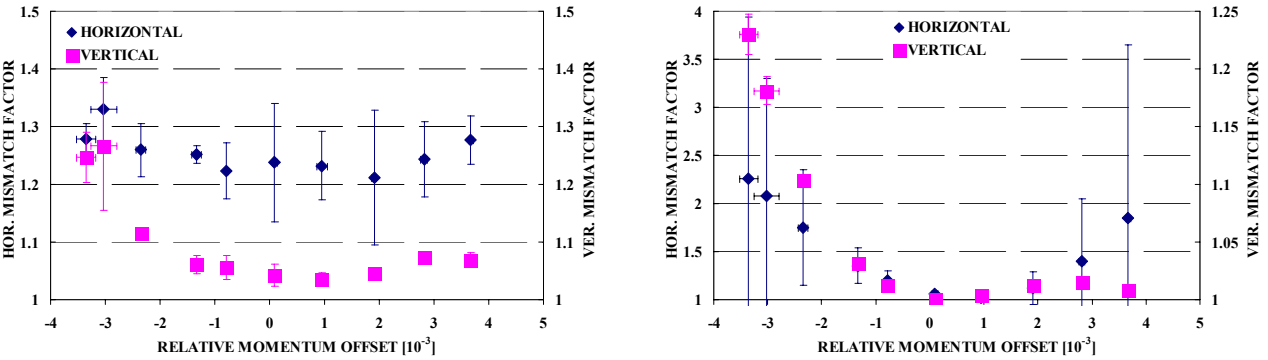

Figure 15.4: Betatron (left) and dispersion (right) mismatch factors after filamentation vs. momentum offset.

A new optics, taking into account these measurements and the new SPS working point has recently been computed in order to reduce the expected mismatch factors further, down to the 5% level (~0.15 μm).

A set of wire scanners is installed in the PS and SPS rings to allow comparative emittance measurements. Measurements performed during 2002 in the PS and SPS confirmed that the blow-up factors derived above represent a pessimistic estimate of the core emittance blow-up. Fig. 15.5 shows the emittance of LHC bunch trains, consisting of 12 or 72 bunches, measured just before extraction in the PS and 10ms after injection in the SPS during 2002 [24]. It is interesting to note that the agreement between the PS and SPS values is particularly good for a bunch train consisting of 12 bunches, for which no significant source of blow-up is expected except injection errors. In Fig. 15.4 the error bars are the rms average of 10 consecutive measurements, except in the case of the measurement in the PS for a bunch population of 0.7×10^{11} protons. In this particular case only one measurement was performed.

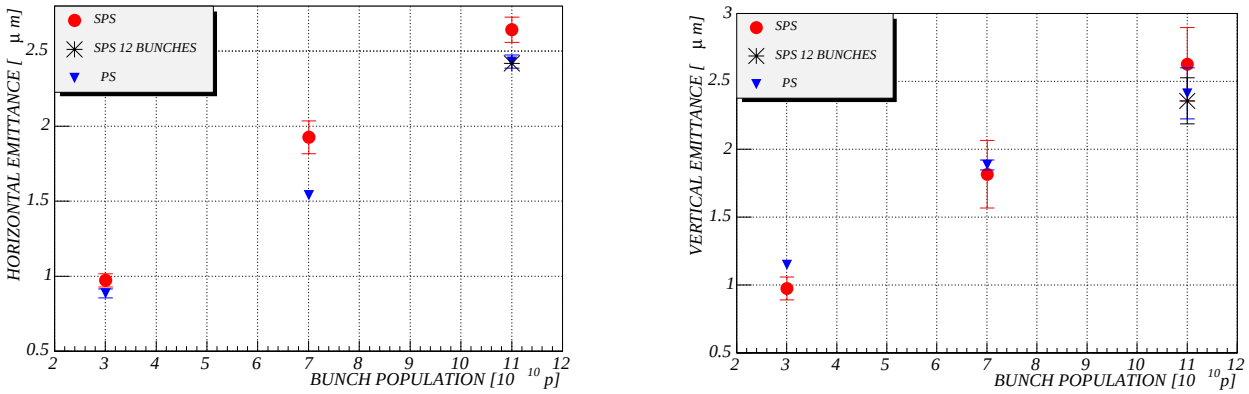

Figure 15.5: Horizontal (left) & vertical (right) emittance comparison for the LHC beam in the SPS and PS with different intensities and number of bunches.

15.3.6 Matching Correction Strategy During LHC Operation

The methods described above allow the measurement of the different static contributions to mismatch. With successive measurements and re-matching of the injection line it should be possible to control the blow-up at injection, after filamentation, to around 5% [17]. These measurements and corrections can only be performed at the beginning of each machine run or during dedicated machine tuning periods, since they demand beams with special characteristics (see Tab. 15.1) and the measurements themselves are time consuming. Further reduction of the mismatch may be obtained by a non-deterministic approach. This would consist of monitoring the beam profile oscillations after injection and minimising the oscillations by trial-and-error trimming of the transfer line matching quadrupoles. Special trim knobs (collections of quadrupole strength trims) can be calculated to give a specific variation of the Twiss or dispersion functions at injection.

The beam size at turn k, σ_k, at a given position in the SPS machine as a function of the betatron and dispersion mismatch is given by:

$$\sigma_k{}^2 = \left(\overline{D}\sigma_{\delta p/p0}\right)^2 + \overline{\beta}\varepsilon\left(H + J_D - 1\right) + \overline{\beta}\varepsilon\left[\sqrt{H^2 - 1}\cos\left[2k\left(2\pi Q\right) + \delta\right] + \left(J_D - 1\right)\cos\left[2k\left(2\pi Q\right) + 2\psi\right]\right] +$$
$$+ 2\overline{D}\sigma_{\delta p/p0}\sqrt{2\overline{\beta}\varepsilon\left(J_D - 1\right)}\cos\left[k\left(2\pi Q\right) + \psi\right]$$

$$\delta = \arctan\left[-\frac{\overline{\alpha}\beta_m - \alpha_m\overline{\beta}}{\beta_m - \overline{\beta}H}\right] \qquad \psi = \arctan\left[-\frac{\Delta D_n}{\Delta D'_n}\right]$$

where $\overline{D}$, $\overline{\alpha}$ and $\overline{\beta}$ are the nominal dispersion and Twiss parameters at the position of the profile monitor and Q is the tune of the SPS machine.

Two matching monitors have been installed in the SPS in positions with and without horizontal dispersion (42194 and 51998) [25,26]. These are both OTR screens (12 μm Ti) with dedicated electronics and can be used to monitor beam size oscillations at injection. Two-dimensional beam profiles can be measured every

eight turns. Having data from positions with and without horizontal dispersion can be used to disentangle the contributions due to dispersion and betatron mismatch, which oscillate with different frequencies. This is not possible in the vertical plane due to the absence of dispersion. The mismatch measurement with the matching monitor is destructive. In fact, although thin, the Ti foils induce some direct blow-up due to multiple scattering and the beam must be aborted after a few tens of turns. For this reason harmonic analysis is difficult to apply.

The effectiveness of the process for reducing the injection mismatch below 5% will depend significantly on the orthogonality of the matching knobs. Studies have been devoted to the possibility of obtaining orthogonal knobs using the available set of quadrupoles and power converters in the injection line. These studies have shown that a complete set of tuning knobs for independent tuning of the Twiss and dispersion parameters cannot be obtained with the present transfer line optics [27,28]. A maximum of six optical matching knobs can be built for independent tuning of the parameters; D_H, D'_H, α_V, β_V, D_V, D'_V at the SPS injection point. Each tuning knob uses the same set of 10 quadrupoles and implies the installation of trim power converters (or trim quadrupoles) in proximity of the quadrupoles QID1011, QID1013, QID1019, QID1025 and QID1027. Numerical simulations confirm that the six knobs are orthogonal and exhibit negligible coupling over a tuning range corresponding to ±5% emittance growth. No satisfactory solution has been found for the parameters α_H and β_H, neither of which can be tuned over any practical range without affecting other parameters. This problem appears to be related to the absence of a dispersion-free region in the horizontal plane [28]. It seems reasonable to assume that 5% emittance growth should be allocated for mismatch at injection due to static errors.

On-line monitoring of the injection mismatch, at least during the pilot injections, could be guaranteed by OTR profile measurements in the injection line with limited emittance growth. With five OTR monitors available it is possible to measure the emittance, the Twiss and the dispersion parameters at one of the monitors if the momentum spread $\sigma_{\delta p/p0}$ of the beam and the transfer matrices between any pair of monitors are known [22]. The momentum spread of the beam can also be measured with the multi-profile analysis method whenever six beam profile monitors are available. A redundancy in the number of beam profile measurements with respect to the number of unknowns is desirable in order to minimise the errors in the measurement [19].

Non-invasive monitoring of the emittance growth at injection can be performed by comparing the emittances measured with the wire scanners installed in the PS and SPS. In the SPS, wire scanners are installed in both non-dispersive and dispersive (in the horizontal plane) regions. This allows a measurement of the transverse emittance and the momentum spread of the beam after capture [24], however the measurement integrates over several turns and, in case of an observed blow-up, it does not provide any information about its origin.

Turn-by-turn non-destructive beam profile monitors are also under investigation. These include a quadrupolar pick-up [29] and an ionisation profile monitor with dedicated fast acquisition electronics [30].

15.4 STATIC ERRORS AFTER INJECTION

The main static sources of emittance growth after injection are related to multipole errors that could reduce the dynamic aperture of the machine. A model of the SPS machine including distributed allowed multipoles in the main dipoles and quadrupoles has been built and has been experimentally validated [9].

Two main ring sextupoles were displaced during the shutdown 2003-2004 in order to restore the original SPS layout and increase the dynamic aperture [31]. The layout has been modified in order to install the two low-beta insertions for collider operation and which is no longer necessary.

The high bunch intensity and the non-uniform distribution of the beam (both in the transverse and longitudinal plane) give rise to a tune spread coming from the direct space charge forces. This means that the beam occupies an area (tune footprint) instead of a point in the tune diagram. This phenomenon is particularly significant at injection. The horizontal and vertical tune spreads of the LHC beam in the SPS at injection are presented in Tab. 15.4 both for the nominal and ultimate intensities.

Table 15.4: Space-charge tune spread in the SPS at injection for the nominal and ultimate intensities.

	ΔQ_H	ΔQ_V
Nominal	-0.041	-0.054
Ultimate	-0.060	-0.079

The working point in the tune diagram must be chosen so as to avoid any overlap of the tune footprint with resonances and, in particular, systematic resonances. In the case of high-intensity machines there are additional considerations which enter into the choice of working point. For large machines, resistive wall is one of the main instabilities affecting the beam. The growth time of this instability depends on the tune of the machine because the real part of the resistive wall impedance depends on the frequency ω: $1/\omega^{1/2}$ (wall thickness >> skin depth) or $1/\omega$ (wall thickness ~ skin depth). In both cases tunes just above the integer are favoured [32].

On the basis of these considerations the coherent tunes $Q_H = 26.185$ and $Q_V = 26.13$ have been chosen for the nominal LHC beam as compared to the tunes, $Q_H = 26.62$ and $Q_V = 26.58$, which are used for fixed-target operation.

Recent studies have shown that operation with high RF voltage at the injection flat-bottom might be required in order to minimize capture losses for the nominal LHC beam with 25 ns spacing. This implies a larger momentum spread and therefore a significant contribution to the vertical tune spread because of the large chromaticity required to fight the electron cloud instability (see Sect. 15.6.1). A new working point (Q_H=26.12 and Q_V=26.185) has been tested in order to avoid any overlap of the tune footprint with the vertical integer stop-band (Q_V=26). Very encouraging results have been obtained. The tune diagrams with the three above-mentioned working points and the systematic (thick lines) and non-systematic (thin lines) resonances from second to fifth order are presented in Fig. 15.6. The integer resonances are not shown.

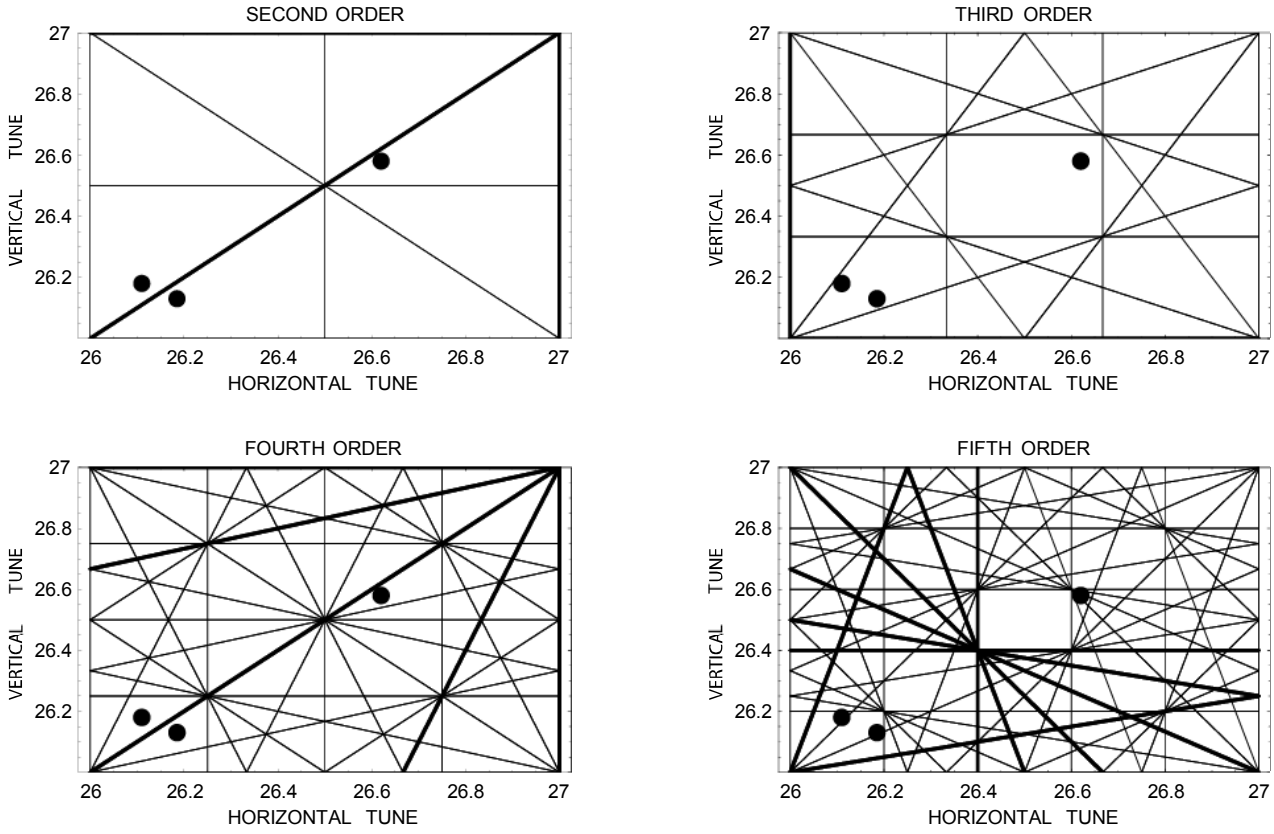

Figure 15.6: SPS working points with systematic and non-systematic second to the fifth order resonances

Table 15.5: Basic parameters of the SPS optics for the nominal LHC beam

	Horizontal plane	**Vertical plane**
Coherent tune	26.185	26.13
Maximum dispersion [m]	4.825	0.015
Maximum β [m]	107.12	107.73
Minimum β [m]	20.05	19.97
Gamma transition γ_{tr}	22.83	
Momentum compaction α_p	1.919×10^{-3}	

The basic parameters for the SPS optics used so far for the LHC beam are listed in Tab. 15.5. The Twiss parameters and dispersion functions for this optics at the injection point are listed in Tab. 15.6.

Table 15.6: Injection conditions of the SPS optics for the nominal LHC beam

	Horizontal plane	**Vertical plane**
β [m]	101.74	21.23
α [1]	-2.293	0.558
D [m]	0.033	0.005
D' [1]	0.009	0.0

15.5 DYNAMIC SOURCES OF EMITTANCE GROWTH

Dynamic sources of emittance growth include all sources of beam oscillations that cannot be predicted and therefore corrected in advance by adequate feed-forward mechanisms. These include:

- Injection errors varying from cycle-to-cycle
- Transverse instabilities.

A feedback system is installed in the SPS to control these perturbing effects. The specifications for such a feedback can be derived, based on the properties of the LHC beam. The additional criteria that the emittance blow-up during the injection process should not exceed 0.15 μm and the blow-up during the remainder of the SPS acceleration cycle should be less than 0.2 μm must also be met [2].

15.5.1 Injection Errors

The dynamic or varying part of the injection errors is due to [33,34]:

- Any ripple in the bending elements of the injection line, or of the PS extraction,
- Any ripple in the PS extraction kicker, or during the SPS injection kicker pulse flat-top,
- The finite rise-time of the PS extraction, or SPS injection kickers.

The emittance increase due to injection errors is caused by the decoherence of the injection oscillation resulting from the tune spread in the beam. Active damping reduces the emittance growth and the deflection strength required depends upon the expected error amplitude, while the extra gain (above the one that is needed for stability) depends upon the tune spread ΔQ. The expected emittance growth $\Delta\varepsilon^*$ for a damper with gain G[1] is [33]:

$$\Delta\varepsilon^* = \frac{\Delta\varepsilon_0{}^*}{\left(1+\frac{G}{2.5\,\Delta Q}\right)^2} \qquad \text{where} \qquad \Delta\varepsilon_0{}^* = \beta\gamma\frac{\Delta X_n^2 + \Delta X_n'^{\,2}}{2}$$

here, $\Delta\varepsilon_0{}^*$ is the emittance growth after filamentation in the absence of a transverse feedback.

Measurements performed in the SPS at 26 GeV/c seem to indicate that space charge plays a dominant role in the decoherence of a kicked beam [34]. In addition, non-linearities can also produce a tune spread and therefore decoherence; however, their contribution is negligible in the SPS. As a result the values of the space charge tune spread listed in Tab. 15.4 can be assumed when evaluating the required extra feedback gain at injection.

The present experience with the LHC beam indicates that residual injection errors due to the ripple of bending magnets in the TT2-TT10 line can induce peak-to-peak first turn trajectory distortions of less than ±1 mm in both planes, after adjustment of the static errors. In the horizontal plane, the contribution of the ripple of the pulse flat-top of the PS and SPS extraction kickers must also be added. For the SPS injection

[1] The gain G is the ratio of the deflection at the output of the feedback to the position at the input, both in normalised units.

kicker a pulse flat-top ripple of ±0.5 % and a kick rise-time of 220 ns have been assumed [33]. Similar normalised values have been taken for the PS extraction kicker [35]. Tab. 15.7 summarises the requirements (above the needs for stability) for the transverse feedback in order to keep the emittance growth due to dynamic injection errors below $\Delta\varepsilon^* = 0.15$ μm.

Table 15.7: Transverse feedback requirements in order to keep the emittance growth due to dynamic injection errors below 0.15 μm for the nominal LHC beam.

	Horizontal plane	**Vertical plane**
$\Delta\varepsilon^*$[μm]	0.15	0.15
$\Delta\varepsilon_0^*$ – bending magnets [μm]	0.28	0.28
$\Delta\varepsilon_0^*$ – SPS injection kicker [μm]	0.25	-
$\Delta\varepsilon_0^*$ – PS extraction kicker [μm]	0.25	-
$\Delta\varepsilon_0^*$ – total [μm]	0.78	0.28
ΔQ	0.041	0.054
Total gain	0.13	0.05

Non-nominal kicker rise-time and/or incorrect pulse synchronisation to the beam can result in bunch-to-bunch injection errors that might require a significant gain up to 20 MHz. For this reason, the aforementioned kicker rise time is mandatory for optimum performance.

15.5.2 Transverse Instabilities

Transverse instabilities are an additional source of emittance growth for the LHC beam. The high bunch intensity, the close spacing and high number of bunches are responsible for the occurrence of single- and coupled-bunch transverse instabilities. The most important ones are:

- Head-tail instability
- Resistive-wall instability
- Electron-cloud instability.

Head-tail instability

The head-tail instability is a single-bunch transverse instability driven by the SPS broadband impedance (see Chap. 17). It was already observed during $p\bar{p}$ operation where bunch intensities comparable to those of the LHC where injected in the SPS at the same injection energy. The most unstable mode is the m = 0 dipole mode. This can be stabilised by adjusting the chromaticity to be slightly positive (above transition). Recent observations and estimates seem to indicate that a fast head-tail instability might develop in the vertical plane for bunch populations close to the ultimate intensity and may require high values of the vertical chromaticity (ξ_V up to 1) to provide sufficient damping.

Resistive-wall instability

The resistive wall impedance drives coupled-bunch instabilities for high intensity beams. These can be observed with the fixed target beam (which almost completely fills the SPS ring) for total intensities above 2×10^{12} protons. For a uniformly filled machine the fundamental modes at 35 kHz (H) and 37.5 kHz (V) are unstable and the transverse feedback is needed to damp them. For a partially filled machine, higher frequency modes (up to 20 MHz) also become unstable although the dominant modes remain the low frequency ones, as shown in Fig. 15.7. The expected growth times for the nominal LHC beam are 40 and 18 turns in the horizontal and vertical planes, respectively. The latter growth times imply a feedback gain of 0.05 in the horizontal plane and 0.11 in the vertical plane [33].

Using octupole magnets to stabilise the LHC beam against the resistive wall instability would generate a tune spread of the order of 0.1 [35]. The octupole strength required is too large to be practical and would

require a higher gain of the feedback in order to keep the emittance growth due to injection errors within the above-mentioned budget.

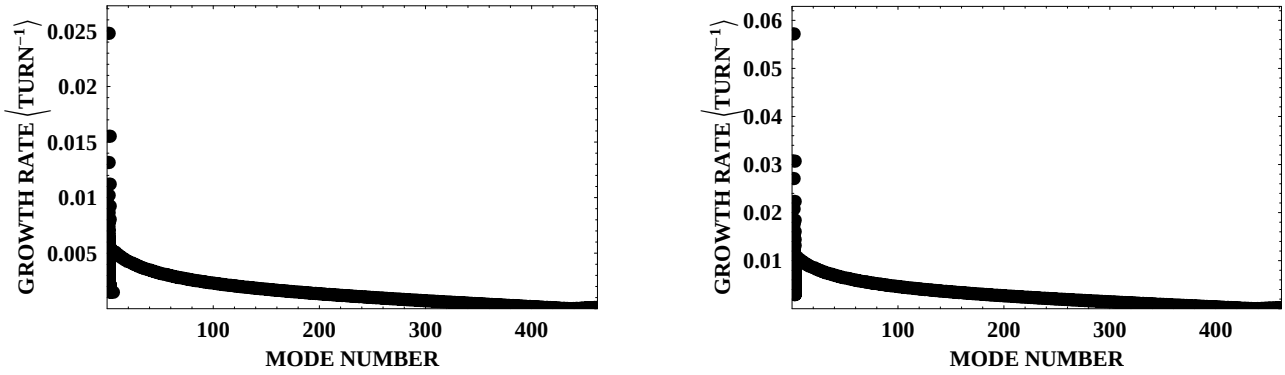

Figure 15.7: Growth rate of the resistive wall instability vs. mode number in the horizontal (left) and vertical (right) plane for the nominal LHC beam.

Electron-cloud instability

The electron cloud induced by the LHC beam in the SPS (see Sec. 15.6) is responsible for strong transverse instabilities. In the horizontal plane a coupled-bunch instability develops in about 40 turns at injection. In the vertical plane a single bunch TMCI-like instability (at about 700 MHz) occurs. In the vertical plane the transverse feedback cannot effectively damp the single bunch instability, since it is at such a high frequency. For the vertical plane high positive chromaticity values are presently the only known only cure capable of stabilising the beam. Unfortunately the high chromaticity leads to a decrease in the decoherence time and therefore imposes even tighter requirements on the feedback gain required to damp time varying injection errors. In the horizontal plane only low-order modes (up to few MHz) are excited and these can be damped by the transverse feedback. The gain required in the horizontal plane is 0.05.

15.5.3 Emittance Conservation During Injection Plateau and Acceleration

The feedback must remain active between consecutive injections during the whole injection plateau and then during the ramp, in order to fight coupled-bunch oscillations driven by the resistive wall and electron cloud instabilities. The beam will oscillate during the cycle up to the observation limit of the system. This limit is determined by the highest noise level in the feedback loop. This persistent oscillation will blow up, or heat, the beam emittance at a rate proportional to square of the tune spread and of the feedback position monitor resolution [33,36]. To meet the requirement of an emittance growth of less than 0.2 μm during the injection plateau and the ramp (i.e. for a total of 19.35 seconds), the average growth rate must be smaller than 0.01 μm/s. This is a pessimistic assumption since the tune spread decreases rapidly with energy in the case where space charge effects dominate.

15.5.4 Requirements for the Transverse Feedback

The requirements for the transverse feedback in terms of gain and normalised kick strength are summarised in Tab. 15.8. The maximum gain must be guaranteed over a bandwidth of a few MHz although the extension to 20 MHz, even with lower gain, allows the system to damp all the coupled-bunch modes for the LHC beam.

The requirements listed in Tab. 15.8 differ from those presented in [2] and take into account the recent experience gained with the LHC beam. In particular, they take into account the additional requirements imposed by the observation of the electron cloud instability in the SPS.

The dynamic range of the digital electronics of the observation part of the transverse feedback can be reduced at the expense of a reduced electronic acceptance. This would imply tighter constraints on the residual orbit distortion after correction and on the acceptable momentum offset.

Table 15.8: Requirements for the transverse feedback for the nominal LHC beam [33,36].

	Horizontal plane	**Vertical plane**
Gain to damp injection errors	0.13	0.05
Gain to damp resistive wall instability	0.05	0.11
Gain to damp electron cloud instability	0.05	-
Total gain	0.23	0.16
Normalised kick strength [$m^{1/2}$]	39×10^{-6}	16×10^{-6}
Resolution of the beam position monitor at $\beta = 100$ m [μm]	11	8
Least Significant Bit resolution [μm]	38	29
Electronic acceptance [mm]	± 19	± 15
Dynamic range [ADC bits]	10	10

15.6 ELECTRON CLOUD EFFECTS IN THE SPS

With the availability of the LHC beam from the pre-injectors in 1999, studies were started to determine the behaviour of the LHC beam in the SPS. From the first tests it became evident that electron multipacting was occurring in the SPS vacuum chambers in the presence of this beam [37]. Although this phenomenon was expected in the LHC because of the large number of photoelectrons produced by synchrotron radiation (10^{-3} photoelectrons/m per proton at 7 TeV), the SPS was thought to be immune since the number of seed electrons was expected to be much smaller, being mainly dominated by ionisation of the residual gas (10^{-7} electrons/m per proton) [38].

Electron multipacting in the SPS is the consequence of the high bunch intensity and the bunch spacing. The electrons accelerated by a bunch may gain enough energy to traverse the vacuum chamber before the next bunch passage and to extract secondary electrons from the chamber walls, in which case the following bunch in turn accelerates these secondary electrons. An exponential growth of the number of electrons occurs if the Secondary Electron Yield (SEY) of the vacuum chamber surface is larger than 1.0 at the energy of the impinging electrons. The energy gained by the electrons depends on the bunch population, bunch length, bunch spacing and on the chamber dimensions. These parameters determine the multipacting threshold. Multipacting is a single-pass phenomenon and has also been observed in transfer lines [19]. In this case, during the passage of the beam, an electron cloud builds-up along the batch until the space charge fields associated with the cloud itself on average cancel the beam field [39].

In the absence of beam the decay time of the electron-cloud might be larger than the beam gap or the revolution period or even last seconds [40]. Fig. 15.8 shows the build-up of the electron cloud along two consecutive batches with nominal spacing (225 ns), as measured with a dedicated electron cloud monitor. The electron cloud developed by the passage of the first batch does not disappear completely during the gap between two consecutive batches and the build-up of the electron cloud in the second batch is faster than in the first.

As a result of the electron bombardment, gas desorption occurs from the vacuum chamber walls and dramatic pressure increases (by more than a factor 100) are observed, mainly in the SPS arcs, preventing stable operation above the multipacting threshold.

The threshold for the onset of the beam-induced multipacting in the SPS has been measured for the LHC beam for 25, 50 and 75 ns bunch spacings. The results are presented in Tab. 15.9 and refer to the arcs. In each case, the data correspond to a single LHC bunch train at injection in the SPS and for an unconditioned surface.

Table 15.9: Threshold for the onset of the electron cloud in the SPS arcs for different bunch spacing for a single LHC bunch train at injection in the SPS.

Bunch Spacing [ns]	N_{bunch} [10^{11}]	# bunches/batch
25	0.3	72
50	0.6	36
75	1.2	24

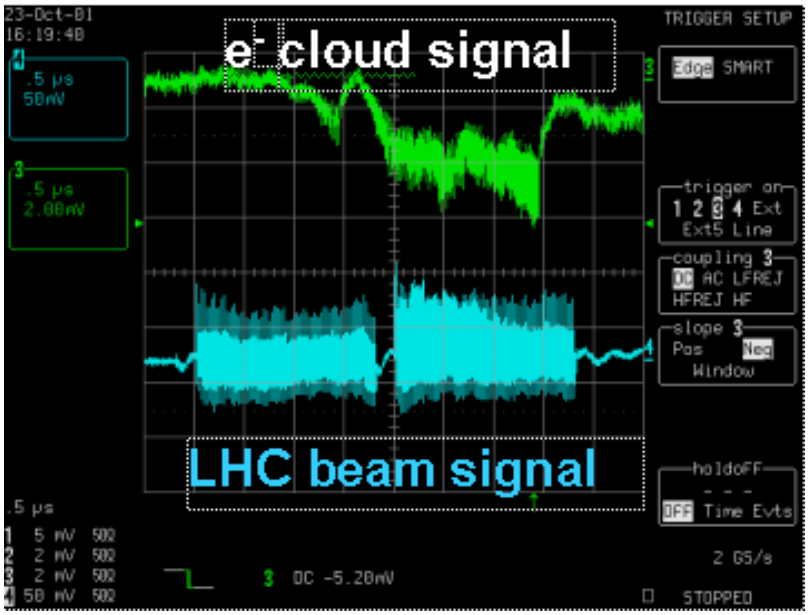

Figure 15.8: Electron cloud build-up along two LHC batches with nominal spacing [41]. The incident electron flux on the wall detected by a shielded pick-up is shown.

In the main dipole magnets (covering about 70 % of the SPS circumference) and above the threshold, the electron cloud surrounds the beam for bunch populations smaller than $0.5\text{-}0.6\times10^{11}$ protons; for larger values, electrons concentrate in two stripes positioned symmetrically with respect to the beam and parallel to the magnetic field lines. At the nominal bunch population or larger, a third stripe centred on the beam also appears [42].

The electron build-up is a strong limitation to the performance of beam instrumentation. A large distortion of the baseline of the signal provided by the high-impedance electrostatic pick-ups of the SPS transverse feedback has been observed [43] in the presence of the LHC beam and this required a modification of the observation part of the feedback, to replace the base-band processing which had been planned initially [2] (see Chap. 14).

Overwhelming noise on secondary emission and ionisation profile monitors in TT2-TT10 also prevents reliable emittance measurement of the nominal LHC beam in the injection line using SEM grids or SEM wires [19]. This leaves the OTR screens as the only reliable device for emittance measurement of the nominal LHC beam in the transfer line.

High voltage electrostatic devices like the electrostatic septa used for the slow extraction of the fixed-target beam to the North and West Areas are also affected by electron multipacting and operation with LHC beams is performed with low cathode voltage and powered ion traps in order to minimise the multipacting in the anodes (see Chap. 12)

15.6.1 The Electron Cloud Instability in the SPS and its Cures

Above the threshold for the onset of electron multipacting, transverse instabilities develop along the batch. These start from the tail and progress towards the head of the batch and result in strong emittance blow-up and even in beam losses. Fig. 15.9 shows the normalised rms emittance measured along a LHC bunch train consisting of 48 bunches a few tens of milliseconds after injection for a bunch population of $N_{bunch} = 0.8 \times 10^{11}$ p, higher than the threshold bunch population of $N_{th} = 0.2 \times 10^{11}$ p. The measurements were taken with the transverse feedback off and with low positive chromaticity ($\xi_H \sim \xi_V \sim +0.05$). The blow-up is particularly evident in the tail of the batch.

For a single batch with nominal bunch population all but the first ten to fifteen bunches are affected by the instability. The number of bunches affected decreases as the bunch intensity decreases. When more batches are injected with nominal batch spacing the instability affects a larger and larger number of bunches in

passing from the first to the last (fourth) batch. These observations are compatible with the measured build-up and decay of the electron cloud density along and between successive bunch trains, shown in Fig. 15.8 [41].

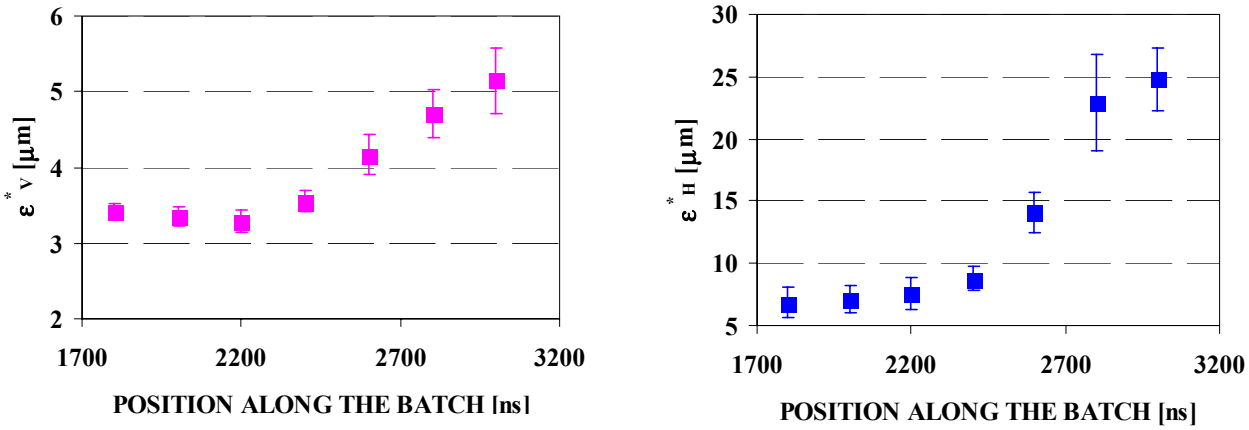

Figure 15.9: Horizontal (left) and vertical (right) rms emittance along the LHC bunch train a few tens of milliseconds after injection for $N_{bunch}>N_{th}$. The origin of the time scale is arbitrary.

The properties of the instability are significantly different in the horizontal and vertical planes. In the horizontal plane it manifests itself as coupled-bunch instability while in the vertical plane a single bunch Transverse Mode Coupling like instability occurs [44].

In the horizontal plane, low order coupled-bunch modes (up to few MHz) are the most unstable and can be damped by the transverse feedback. The rise time of the instability is of the order of 40 turns and is only weakly dependent on the bunch population. An additional gain of 0.05 must be allocated for damping the electron cloud instability in the horizontal plane (see Tab. 15.8). The rise time has been measured at different energies and it increases linearly with the momentum of the beam in the same way as for the resistive wall instability.

The vertical electron cloud instability is of a single bunch type: a measurement of the bunch-by-bunch position over several turns does not show any phase correlation among subsequent bunches. The instability mainly affects the tail of the batch and the rise time decreases with increasing bunch population (N_{bunch}). The maximum amplitude of oscillation is reached after about 600 turns for $N_{bunch} = 3\times10^{10}$ protons and in 300 turns for 5×10^{10} protons. A vertical motion inside the bunch at frequencies of about 700 MHz has been observed which may be associated with the electron oscillation frequency and possibly with additional external impedance. The single-bunch instability observed cannot be damped by the transverse feedback that can only detect and correct dipole modes. Running at high chromaticity (ξ_V up to 1.5) is the only cure found so far to fight the electron cloud instability in the vertical plane. Landau damping by octupoles requires impractical values of the detuning with amplitude. This cure has been tried but it resulted in significant blow-up and poor beam lifetime [45]. Another possible remedy for the vertical single bunch instability might be to use linear coupling [46].

15.6.2 Cures for the Electron Cloud Effects in the SPS

Though cures exist to fight the electron cloud transverse instabilities a remedy to minimise electron multipacting is mandatory in order to eliminate or minimise the electron cloud effects previously mentioned and in particular the dynamic pressure increase.

Solenoid fields [47] or clearing electrodes [48] can locally suppress electron multipacting but these solutions are not applicable for the SPS where multipacting occurs mainly in the main dipoles. Other methods consist of reducing the SEY of the vacuum chamber surface [49]. Methods include:

- Changing the surface composition by glow discharge treatments,
- Depositing TiN films, or Non Evaporable Getters such as TiZrV [50],
- Electron bombardment (or ‘scrubbing’).

The latter process has been thoroughly studied at CERN [51] and it has been recently observed in the SPS [52]. A reduction of the Secondary Electron Yield from 2.3 to 1.6 has been obtained after a few days of continuous dedicated running of the SPS with the nominal LHC beam at injection. A further reduction to around 1.5 has been achieved after several hours of running with the nominal LHC beam up to 450 GeV/c. The thresholds for the onset of the beam-induced multipacting have correspondingly increased from 0.3×10^{11} p/bunch to 1.0×10^{11} p/bunch in the arcs and from 0.5×10^{11} p/bunch to 1.3×10^{11} p/bunch in the straight sections. The dynamic pressure increase in the presence of LHC beams was reduced by a factor 10^4 in the same period. Some de-conditioning (i.e. an increase of the SEY) is observed if operation with the LHC beam is interrupted or the bunch intensity is reduced, though the initial SEY can be rapidly recovered if the initial beam conditions are re-established. Experience shows that the electron cloud activity cannot be fully suppressed and the final threshold intensities and SEY depend on the operational conditions of the machine.

For the above reason the measures to fight the electron cloud transverse instability mentioned above must be implemented to obtain nominal beam parameters.

REFERENCES

[1] X. Altuna et al., *Acceleration of High Intensity Proton Beams in the SPS*, PAC 1999, New York, pp. 2617-2619 and CERN-SL-99-028-OP.

[2] P. Collier, ed., *The SPS as LHC Injector for LHC – Conceptual Design*, CERN-SL-97-07-DI.

[3] MAD model for the TT2-TT10 line.

[4] G. Arduini, M. Giovannozzi, K. Hanke, J.-Y. Hemery, M. Martini, *MAD and Beam Optics Description of the TT2/TT10 Transfer Lines - Part I: Optics without Emittance Exchange Insertion*, CERN PS-Note-98-014 CA, CERN-SL-Note-98-040 OP.

[5] MAD model for the PS ring.

[6] MAD model for the SPS ring.

[7] G. Arduini, M. Giovannozzi, K. Hanke, J.-Y. Hemery, *Study of the TT2/TT10 Transfer Line Optics via Transfer Matrix Measurement*, CERN-SL-Note-98-058 MD, CERN PS-Note-98-020 CA.

[8] R. Cappi, M. Giovannozzi, M. Martini, E. Métral, G. Métral, R. Steerenberg, A.-S. Müller, *Optics Studies for the CERN Proton Synchrotron Machine: Linear and Non-linear Modelling using Beam Based Measurements*, CERN-AB-2003-017-ABP.

[9] G. Arduini, F. Zimmermann, A. Faus-Golfe, N. Iida, R. Tomas, *2002 Non-linear Optics Measurements and Modelling for the SPS at 26 GeV*, CERN-AB-Note-2003-025 MD.

[10] I. Kirsten, D. Manglunki, M. Martini, *Trajectory and optical parameters in a non-linear stray field*, CERN-PS-96-024.

[11] D. Manglunki, M. Martini, *Beam Optics Modelling at CPS Extraction throughout a non-linear fringe field*, CERN-PS-97-015-CA.

[12] G. Arduini, P. Raimondi, *Transverse emittance blow-up due to injection errors*, CERN-SL-Note-99-022-SLI.

[13] J. Wenninger, *SPS Optics Measurements with Closed with Closed Orbits*, SL Seminar – 04/04/02.

[14] G. Arduini, P. Collier, C. Niquille, L. Normann, *Measurement of the Circumference and of the Central Frequencies at 26 and 450 GeV in the SPS*, CERN-SL-MD Note 257.

[15] G. Arduini, C. Arimatea, T. Bohl, P. Collier, K. Cornelis, J. Wenninger, *Energy Calibration of the SPS at 450 GeV/c with Proton and Lead Ion Beams*, CERN-AB-Note-2003-014 OP.

[16] H. Schmickler, G. Vismara, *A logarithmic processor for Beam Position Measurements applied to a Transfer Line at CERN*, CERN-SL-2001-023-BI.

[17] G. Arduini, *Mismatch Measurements*, CERN/SL-99-007 DI, p. 103-109.

[18] K. Hanke, *Betatron Matching and Dispersion Matching*, CERN/SL-99-007 DI, p. 110-115.

[19] R. Cappi, M. Giovannozzi, E. Métral, G. Métral, G. Rumolo, and F. Zimmermann, *Electron cloud build-up and related instability in the CERN Proton Synchrotron*, Phys. Rev. ST Accel. Beams 5 094401.

[20] R. Jung, *Single Pass Optical Profile Monitoring*, CERN-AB-2003-064-BDI.

[21] Y.-C. Chao, *New Results on TT2-TT10 Matching*, CERN-SL-2001-003 DI, p. 44-55.

[22] G. Arduini, M. Giovannozzi, K. Hanke, D. Manglunki, M. Martini, *New Methods to Derive the Optical and Beam Parameters in Transport Channels*, Nucl. Instrum. Methods Phys. Res., A 459 (2001) 16-28.

[23] C. Carli, G. Cyvoct, M. Giovannozzi, E. Métral, G. Métral, R. Steerenberg, *Emittance Exchange By Crossing A Coupling Resonance*, CERN-PS-2002-020-AE.
[24]G. Arduini, Y.-C. Chao, M. Giovannozzi, D. Jacquet, J. Klem, D. Manglunki, M. Martini, G. Métral, F. Roncarolo, *Summary of the TT20/TT10 Transfer Line Studies in the Years 2001 and 2002*, CERN-AB-Note-2003-086 (ABP).
[25] C. Bovet, J. Camas, R.-J. Colchester, G. Ferioli, J.-J. Gras, R. Jung, J.-M. Vouillot, *The OTR screen betatron matching monitor of the CERN SPS*, CERN-SL-99-050-BI.
[26] C. Bovet, R. Jung, *A new Diagnostic for Betatron Phase Space matching at Injection into a circular Accelerator*, CERN-SL-96-034.
[27] G. Arduini, K. Hanke, *Tuning Knobs for the PS-SPS Transfer Line*, CERN-SL-99-021-OP.
[28] N. Iida, G. Arduini, F. Zimmermann, *Optics Matching Knobs for Injection from PS to SPS (TT2/TT10) Constructed by SAD Code*, CERN-SL-Note-2002-035 MD.
[29] A. Jansson, *Non-Invasive Measurement of Emittance and Optical Parameters for High-Brightness Hadron Beams in a Synchrotron*, CERN-PS-2001-014-OP.
[30] G. Ferioli, C. Fischer, J. Koopman, F. Roncarolo, *Beam Studies Made with the SPS Ionisation Profile Monitor*, CERN-AB-2003-066-BDI.
[31] G. Arduini, A. Faus-Golfe, R. Tomas, *Study of the effect of restoring the original SPS lattice sextupoles configuration on single-particle stability*, CERN-AB-Note-2003-042 ABP.
[32] J. Gareyte, *Observation and Correction of Instabilities in Circular Accelerators*, CERN-SL-91-09-AP.
[33] L. Vos, *Mismatch, Damping and Emittance Growth*, CERN-SL-99-007 DI, p. 99-102.
[34] L. Vos, *Transverse emittance blow-up from dipole errors in proton machines*, CERN-LHC-Project Report 193.
[35] L. Vos, *Damping of coherent oscillations*, CERN-SL-96-66 (AP).
[36] D. Boussard, *Evaluation of Transverse Emittance Growth from Damper Noise in the Collider*, SL-Note 92-79 (RFS) and LHC Note 218.
[37] For a general overview on the measurements and simulations on the electron-cloud build-up and its effects see: *Proceedings of ECLOUD'02 – Mini-Workshop on Electron-Cloud Simulations for Proton and Positron Beams*, CERN-2002-001.
[38] F. Zimmermann, *Electron-Cloud Simulations for SPS and LHC*, CERN-SL-2000-007-DI, p. 136-149
[39] F. Zimmermann and G. Rumolo, *Two-Stream Problems in Accelerators*, CERN-SL-2001-057 (AP).
[40] G. Arduini, *Electron Cloud and Ion Effects*, EPAC'02, Paris, and CERN SL-2002-056-OP.
[41] J.-M. Jimenez, et al., *Electron Cloud with LHC-Type Beams in the SPS: A Review of Three Years of Measurements*, LHC Project Report 632 (2003).
[42] J.-M. Jimenez, et al., *Electron Cloud Studies and Analyses at SPS for LHC-Type Beams*, PAC'03, Portland.
[43] W. Höfle, *Observation of the Electron Cloud Effect on Pick-Up Signals in the SPS*, CERN-SL-2000-0007 DI, p. 112-118.
[44] G. Arduini, K. Cornelis, W. Höfle, G. Rumolo, F. Zimmermann, *The Electron Cloud Instability of the LHC Beam in the CERN SPS*, PAC'03, Portland and CERN-LHC-Project-Report-637.
[45] G. Arduini, *Observations on Transverse Instabilities*, CERN-SL-2001-003-DI, p. 125-134.
[46] E. Métral, *Effect of Bunch Length, Chromaticity and Linear Coupling on the Transverse Mode-Coupling Instability due to the Electron Cloud*, CERN-2002-001, p. 211-218.
[47] H. Fukuma, *Electron Cloud Effects at KEKB*, CERN-2002-001, p. 1-9.
[48] R. Macek, *Possible Cures for Electron Cloud Problems*, CERN-2002-001, p. 259-268.
[49] N. Hilleret et al., *Ingredients for the Understanding and the Simulation of Multipacting*, CERN-SL-2000-007 DI, p.130-135.
[50] B. Henrist et al., *The secondary electron yield of TiZr and TiZrV non-evaporable getter thin film coatings*. Appl. Surf. Sci., 172(2001), p.95 and references therein.
[51] N. Hilleret at al, *The Variation of the Secondary Electron Yield and of the Desorption Yield of Copper under Electron Bombardment: Origin and Impact on the Conditioning of LHC*, EPAC'02, Paris, p. 2553-2555.
[52] J.-M. Jimenez et al., *Electron Cloud Studies and Beam Scrubbing Effect in the SPS*, LHC-Project-Report 634.